CrossMark

Natural Volcanic Tuff-Based Geopolymer for Zn Removal: Adsorption Isotherm, Kinetic, and Thermodynamic Study

Kamel K. Al-Zboon · Bashar M. Al-smadi · Sajedh Al-Khawaldh

Abstract Natural volcanic tuff was used for the synthesis of geopolymer and then for the removal of Zn^{+2}. The characteristics of the natural volcanic tuff and the synthesized geopolymer were determined by X-ray diffraction (XRD), X-ray fluorescence (XRF), Fourier transform infrared (FTIR), and scanning electron microscopy (SEM). Results referred that the synthesized geopolymer had a higher efficiency uptake of 97.7 % as against 78.5 % for the natural volcanic tuff. The uptake capacity of geopolymer for Zn^{+2} adsorption increased with increasing temperature in the studied range of 25–45 °C, contact time up to 30 min, pH up to 7, and initial concentration up to 160 ppm, while it decreased with an increase in geopolymer dosage. The isotherm study showed best fit on Langmuir and Radlich-Peterson models. The maximum uptake capacity obtained from Langmuir model increased from 14.7 to 17.63 mg/g as the temperature increased from 25 to 45 °C. The pseudo-second-order model showed the best fitness for the experimental data followed by intraparticle diffusion model. The adsorption process can be characterized as endothermic, homogeneous, spontaneous, irreversible, physical, and a high adhesion of the ions to the geopolymer surface. The results obtained buttressed the feasibility and applicability of producing geopolymer from natural volcanic tuff for the removal of heavy metals.

Keywords Geopolymer · Volcanic tuff · Adsorption · Zinc (Zn) · Model · Thermodynamic

1 Introduction

The main sources of zinc discharged into the environment are from mining operations, galvanizing plants, coal combustion, pharmaceuticals, paints, pigments, insecticides, cosmetics, rubber tire wear, wastewater, and phosphate fertilizers (Salim et al. 2003; Wahi et al. 2010). The tremendous increase in the use of Zn in industries has resulted in a high discharge of this metal into the environment causing the associated adverse impacts on nature and human health. Although zinc is considered as one of the most important base metals necessary for metabolic processes in the body, recent studies have increasingly shown that free ionic zinc (Zn^{+2}) is a potent killer of neurons, glia, and other cell types (Nriagu 2007). Direct exposure to zinc can cause many health problems through inhalation (fever, dry throat, chills, gastroenteritis, substernal chest pain, and cough), ingestion (nausea, vomiting, and diarrhea), dermal contact (ulceration, blistering, and permanent scarring), and ocular (strong eye irritants, pain, erythema, edema and burns, iritic, hyperemia, hemorrhaging, bullous keratopathy, glaucoma, and cataract formation). Zinc also has long-term effects, which include neurotoxicity,

K. K. Al-Zboon (✉)
Department of Environmental Engineering, Al-Huson University College, Al-Balqa Applied University, P.O. Box 50, Huson 21510 Irbid, Jordan
e-mail: alzboon@bau.edu.jo

B. M. Al-smadi · S. Al-Khawaldh
Department of Civil Engineering Faculty of Engineering and Technology, University of Jordan, Amman, Jordan

Springer

hepatotoxicity, hepatic toxicity, cardiovascular toxicity, and hemotoxicity (Nriagu 2007; Plum et al. 2010). Due to its toxicity, OSHA determined the permissible exposure limit for zinc oxide fume in workplaces to be 5 mg/m^3 for 8 h/day (OSHA 2015).

The growing interest in human health and clean environment triggered researchers to create and develop different methods and technologies for the removal and extraction of heavy metals from industrial stream, zinc is one these considerable metals. Traditional methods of Zn removal include precipitation, coagulation, ion exchange, electrodialysis, ultrafiltration, solvent extraction, activated carbon adsorption, or electrochemical deposition. Recently, attention was shifted toward low cost treatment methods such as the use of fly ash (Agarwal et al. 2014), tea factory waste (Wasewar et al. 2008, 2009), gyrolite (Baltakys et al. 2012), plant leaves (Salim et al. 2003), rice bran (Abdul Kadir et al. 2013), sago wastes (Wahi et al. 2010), kaolin (El-Eswed et al. 2012; Meroufel et al. 2013), almond husks (Hasar et al. 2003), phosphogypsum (Chafik et al. 2014), micro-algal species (Chong et al. 2000), and geopolymer (El-Eswed et al. 2012; Chaudhary et al. 2012).

Geopolymer showed superior capacity in the removal and immobilization of heavy metals, and as a result, it got a great attention as a valuable material for the removal of Cd, Ni, Pb(II), Cu(II), and Zn (Ahmaruzzaman 2010). There are few researchers that used geopolymer made with different materials for Zn removal. El-Eswed et al. (2012) used geopolymer-based kaoline and zeolite, and they obtained good removal efficiency for Zn up to 0.4 mmol/g at a ratio of 150:50 zeolite/kaolin, and the geopolymer had a higher removal efficiency for small-sized metal ions like Cu, Ni, and Zn than for large ones like Cd and Pb (El-Eswed et al. 2012). Geopolymer produced from solid waste incineration ash showed good immobilization of Zn (0.07 mg/l), with better results obtained for Pb, Cd, and Mn (0 mg/l) (Lancellotti et al. 2015). Chaudhary et al. (2012) used geopolymer-based fly ash and they found that Zn was immobilized up to 100 % while other metals like Pb, Fe, Mn, and Cu were in the range of 80–99 % immobilization. Geopolymer-based fly ash and blast furnace slag were successfully used for immobilization of Zn. and a good result of 0.133 mg/l at a pH of 8.75 was achieved (Nikolići et al. 2013). Chawakitchareon and Veesommaia (2013) used geopolymer mortar made of silica waste and pure alumina from waste material to

remove heavy metals. The analysis of heavy metal in leachate obtained from waste extraction test revealed that chromium had a value of 1.702 mg/l, while lead, copper, and zinc had values less than 0.1 mg/l.

Studies carried out revealed that geopolymer adsorption capacity is affected by many parameters such as the composition of adsorbent, dosage of adsorbent, pH, contact time, initial concentration of contaminant, and temperature (Al-zboon et al. 2011; Nikolići et al. 2013; Harja et al. 2013; Kumar et al. 2014; Srivastava et al. 2008).

Different materials have been used to produce geopolymer such as fly ash (Li et al. 2006; Al-zboon et al. 2011; Al-Harahsheh et al. 2015), metakaolin (Cheng et al. 2012; Ferone et al. 2013), rice husk ash (Detphan and Chindaprasirt 2009), kaolin (van Jaarsveld et al. 1989), slag (Astutiningsih and Liu 2005), stilbite (Xu et al. 2001), zeolite (El-Eswed et al. 2012), calcined clay (De Weerdt 2011), albite (Xu et al. 2002), and municipal solid waste incinerator fly ash (Lancellotti et al. 2015).

Jordan has huge reserves of volcanic tuff with more than two billion tons of reserves that were estimated in many locations in the northeast and southern parts of Jordan (Al-Zboon and Al-Zou'by 2015). Since its discovery in 1987, considerable researches have been conducted to determine the characteristics of this material as well as its applicability. Due to its availability, high porosity, high efficiency as an adsorbent and ion exchanger, and its low cost, many researchers used it in water and wastewater treatment (El-Eswed and Yousef 2012; Ali and El-Bishtawi 1997; Almjadleh et al. 2014; Al-Shaybe and Khalili 2009; Al-Zou'by Jehad et al. 2013).

In this study, natural volcanic tuff material was collected from Artin in the northeast of Jordan and used to produce geopolymer. This work examines the possibility of using highly available, natural, and low-cost new material for geopolymer production. The geopolymer produced could be used in many environmental and industrial applications such as concrete production and treatment of water, wastewater, and gases.

2 Materials and Methods

2.1 Materials

Two cubic meters of volcanic tuff were collected from Jabal Artin (30 km NE of Al Mafraq), which was then

reduced to the testing size by quartering dividing method. They were grinded gently in a pestle and mortar and sieved for different particle size fractions. The particle size <45 μm was selected for geopolymer synthesis (Wang et al. 2007; Al-zboon et al. 2011). Working solutions of zinc were prepared by diluting 1000-ppm metal stock solutions with distilled water. Zinc nitric acid (HNO_3) and sodium hydroxide (NaOH) solutions were made by Merck- Germany; all reagents used were of analytical grade.

2.2 Instrumentation

X-ray diffraction (XRD) analysis of volcanic tuff and geopolymer samples was performed by the use of a diffractometer (Shimadzu XRD-6000), where data were collected at 2 with scanning range of 5–70°, a step size of 0.02°, and a scanning speed of 2.0°/min. The chemical compositions of samples were obtained using X-ray fluorescence (XRF) spectrometer (Shimadzu XRF-1800). Zn concentration was determined by inductively coupled plasma optical emission spectroscopy (ICP-OES) on Shimadzu ICPS-7510 model. The shape and surface morphology of the volcanic tuff and geopolymer samples were examined with a Superscan SSX series (Shimadzu scanning electron microscope (SEM), Japan) scanning electron microscope using powered samples. Infrared adsorption spectra of samples were recorded using Fourier transform infrared (FTIR) spectrophotometer (Shimadzu FTIR-IRTracer-100) with infrared range of 400–4500 cm^{-1}. pH meter model inoLab® pH 7110 from WTW was used for pH measurements and was calibrated at 20 °C using two buffer solutions (potassium hydrogen phthalate at pH = 4.0 and potassium dihydrogen phosphate at pH = 7.0). The mass measurement of samples was carried out using analytical balance (Shimadzu ATX124) with a minimum display of 0.10 mg and repeatability <0.1 mg. For thermodynamic study, a shaker equipped with a digital thermostat was used to regulate the temperature.

2.3 Geopolymer Synthesis

Geopolymer mix was prepared by adding the volcanic tuff to the NaOH solution (14 M) as an activator with constant mass ratio of 1:1.25. The same ratio was successfully used by Al-zboon et al. 2011. The most common activator is a mixture of water, NaOH, KOH, and sodium silicate. It was found that NaOH is better than

KOH for geopolymer progress and strength (Abdul Rahim et al. 2014). During the process of mixing, the tuff materials (<45 μm) and NaOH geopolymer paste started to form, which culminated in a homogenous mixture after 15 min. Thereafter, the mixtures were casted into two layers in polypropylene cylinders (30 × 60 mm) where each layer was vibrated for 30 s using ultrasonification (Alvarez-Ayuso et al. 2008). The vibration of the geopolymer paste was aimed at deforming the geopolymer body, while ultrasonification process enhances the dissolution of the Al–Si material in the alkaline solution (Alvarez-Ayuso et al. 2008). The paste was then poured into a cylindrical container and reset for 2 days for curing purpose. Usually, after 2 days of reset period, slight increase in geopolymer strength was noticed (Hardjito et al. 2005). The geopolymer specimens were then cured at a temperature of 105 °C for 2 days in an oven. Due to the increased temperature, polymerization became more rapid. Higher curing temperature resulted in a higher compressive strength, and 60–100 °C gave the highest compression strength (Al Bakri et al. 2012; Mane and Jadhav 2008) whereas higher curing temperature did not increase the compressive strength (Rangan 2008). After the curing period, the samples were removed from the oven and kept at room temperature for 3 days (Van Jaarsveld et al. 1997). The geopolymer formed was washed with distilled water three times to ensure that all excess sodium hydroxide is removed. After drying, the synthesized geopolymer bodies were crushed and its size reduced to less than 200 μm for experimental purpose (Izquierdo et al. 2009).

2.4 Adsorption Performance Indicators

Many parameters were used to determine the efficiency of the adsorption process such as removal efficiency, uptake capacity, and distribution coefficient.

2.4.1 Uptake Efficiency

The uptake efficiency (E) was calculated using the following equation (Al-zboon et al. 2011):

$$E = \frac{Co - Ce}{Co} \times 100 \ \% \tag{1}$$

where Co is the initial concentration of Zn^{2+} (ppm) and C_e is the residual concentration of Zn^{+2} ion in the solution after equilibrium (ppm).

2.4.2 Uptake Capacity

The uptake capacity of geopolymer for Zn was calculated as follows (Al-zboon et al. 2011):

$$q = \frac{(Co - Ce)XV}{m} \times 100 \ \% \qquad (2)$$

where q is the amount of Zn^{2+} uptake by synthesized geopolymer (mg Zn/g of geopolymer), V is the volume of the solution (L), and m is the geopolymer dose (g).

2.4.3 Partition Coefficient, K_d

The partition (or distribution) coefficient, K_d is a measure of sorption of contaminants to solid and is defined as the ratio of the quantity of the adsorbate adsorbed per unit mass of solid to the amount of the adsorbate remaining in solution. K_d was calculated using laboratory batch method as shown in the following equation (EPA 1991):

$$K_d = \frac{(Co - Ce)XV}{Co \times m} \times 100 \ \% \qquad (3)$$

2.5 Factors Affecting Uptake Efficiency

The impact of geopolymer dosage, pH, contact time, temperature, and initial concentration on the efficiency

of Zn^{+2} uptake by geopolymer was investigated as illustrated in Table 1. For each set, batch sorption tests were carried out using 50 ml of Zn^{2+} solution with an initial concentration of 1000 ppm. The parameters being considered were investigated under variable ranges (geopolymer dose = 0.03–1.0 g, pH = 1–8, contact time = 5–180 min, temperature = 25 to 45 °C, and zinc concentration = 4–160 ppm). In each experiment, the selected dose of geopolymer was added to the solution containing a specified concentration of Zn^{2+} under a certain pH and temperature. The solution was then shaken for a specified predetermined period. After that, the liquid portion of the solution was removed from the solid by centrifugation followed by filtration with Whatman filter paper no. 42. The filtrate was analyzed by ICP to determine the concentration of Zn^{+2} in the supernatant solution.

2.6 Adsorption Isotherms

Batch equilibrium technique was used to study the adsorption isotherms of Zn^{2+} on the synthesized geopolymer. Different concentrations of Zn^{2+} were added to a constant dose of geopolymer (0.4 g) at different temperatures (25, 35, 45 °C) and different pH (5, 6, and 7). The mixture was shaken for 120 min, after which it was filtered, and the concentration of Zn^{2+} was determined by ICP.

Table 1 Experimental conditions for each set of experiments

Investigated parameter	Values of investigated parameter	Constant parameters
Geopolymer dosage	0.03, 0.05, 0.10, 0.2, 0.30, 0.40, 0.50, 0.60, 1.00	pH = 7 Temp = 25 °C Contact time = 120 min Initial concentration = 100 ppm
Contact time	5, 10, 15, 30, 60, 120, 180	pH = 7 Temp = 25 °C Initial concentration = 100 ppm Geopolymer dosage = 0.4 g
Temperature	25, 35, 45	pH = 7 Contact time = 120 min Initial concentration = 100 ppm Geopolymer dosage = 0.4 g
Initial concentration	10, 20, 40, 60, 80, 100, 120, 140, 160	pH = 7 Temp = 25 °C Contact time = 120 min Geopolymer dosage = 0.4 g

The results obtained from the isotherm study were used to evaluate the applicability of six isotherm models (Table 2) in describing the absorption process. Langmuir's model assumed homogenous and monolayer adsorption process, whereas Freundlich's model assumed multilayer adsorption with non-uniform distribution of adsorption heat and affinities over the heterogeneous surface (Foo and Hameed 2010). The Radlich-Peterson adsorption isotherm has three parameters (K_{rp}, a_{rp}, β) and incorporates the features of Langmuir and Freundlich isotherms into a single equation (Sampranpiboon et al. 2014).

2.7 Error Analysis

The coefficient of correlation (R^2) is usually used to evaluate the applicability of the model to predict the experimental data, but R^2 does not represent the value of the errors in the isotherm model. To evaluate the fitness of the isotherm model to the experimental data, two indicators were used, the mean square error (MSE) and chi-square test (χ^2) as determined by the following equations (Sampranpiboon et al. 2014):

$$\mathrm{MSE} = \frac{1}{n}\sum_{n=1}^{n}(q\exp - q\mathrm{cal})^2 \tag{4}$$

$$\chi^2 = \frac{\sum_{n=1}^{n}(q\exp - q\mathrm{cal})^2}{q\mathrm{calc}} \tag{5}$$

where q_{exp} and q_{cal} represent the experimental and calculated uptake values, respectively (mg/g).

2.8 Kinetic of Adsorption

Three time-dependent models were applied to explain the mechanism of the absorption process. They are Lagergren pseudo-first-order, pseudo-second-order, and intraparticle diffusion model. The general forms of the three models are shown in the following equations, respectively (Amenaghawon 2013):

$$(q_e - q_t) = \mathrm{Ln}q_e - k_1 t \tag{6}$$

$$\frac{t}{q_t} = \frac{1}{k_2(q_e)^2} + \frac{t}{q_e} \tag{7}$$

$$q_t = k_3 \times t^{0.5} + I \tag{8}$$

where q_e and q_t are the adsorption capacity at equilibrium and at time t, respectively (mg/g), and k_1, K_2, and K_3 are the rate constant of the three models, respectively (min^{-1}). k_1, K_2, and K_3 values can be obtained by plotting a graph of $\ln(q_e - q_t)$ against t, t/q against t, and q_t against $t^{0.5}$, respectively.

2.9 Thermodynamic Study

The thermodynamic experiments were carried out at different temperatures (25, 35, 45 °C) and pH values (5, 6, 7). Thermodynamic parameters, enthalpy (ΔH_o, kJ/mol), and entropy (ΔS, kJ/mol) (J/K/mol) were determined by the following equations (Misra et al. 2003):

$$\ln K_d = (\Delta So/R) - (\Delta Ho/RT) \tag{9}$$

where T and R represent the temperature in Kelvin and the gas constant, respectively. A graph plot of $\ln K_d$ against $1/T$ gives a slope of $\Delta H_o/R$ and an intercept of $\Delta S_o/R$, from which ΔS_o and ΔH_o can be determined.

Table 2 Used isotherm models

Model	Equation	Plotting	Obtained constant	References
Langmuir type 1	$\frac{c_e}{q_e} = \frac{1}{qm}c_e + \frac{1}{Kaqm}$	C_e/q_e vs C_e	K_a, q_m	Armagan and Toprak (2012)
Langmuir type 2	$\frac{1}{q_e} = \left(\frac{1}{Kaqm}\right)\frac{1}{c_e} + \frac{1}{qm}$	$1/q_e$ vs $1/C_e$	K_a, q_m	Armagan and Toprak (2012)
Langmuir type 3	$qe = qm - \left(\frac{1}{ka}\right)\frac{qe}{Ce}$	q_e vs q_e/C_e	K_a, q_m	Armagan and Toprak (2012)
Langmuir type 4	$\frac{qe}{Ce} = Kaqm - Kaqe$	q_e/C_e vs q_e	K_a, q_m	Armagan and Toprak (2012)
Freundlich	$\log(qe) = \log(Kf) + \frac{1}{n}\log(Ce)$	$\log q_e$ vs $\log C_e$	K_f, n	Al-zboon et al. (2011)
Radlich-Peterson	$\frac{C_e}{q} = \frac{1}{K_{rp}} + \frac{arp}{K_{rp}} \times Ce^{\beta}$	C_e/q_e vs $C_e{}^{\beta}$	K_{rp}, a_{rp}, β	Solomon Samu et al. (2012)

The change in Gibbs free energy ($\Delta G°$, kJ/mol) was calculated as follows:

$$\Delta Go = \Delta Ho - T\Delta So \qquad (10)$$

3 Results and Discussions

3.1 Characterization of Volcanic Tuff and Geopolymer Samples

Volcanic tuff and geopolymer samples were characterized using XRD, XRF, FTIR, and SEM.

3.1.1 The XRD Characterization

The XRD pattern showed that the volcanic tuff sample is rich in phillipsite followed by chapazite. The high ratio of CaO in the examined sample (Table 3) supported the presence of calcium phillipsite and calcium chapazite (Al-Harahsheh et al. 2014). A considerable amount of non-zeolitic impurity was detected which was mainly dioposide ($CaMgSi_2O_6$) and calcite ($CaCO_3$). Similar results with minor differences had been obtained by many researchers (Almjadleh et al. 2014; Ali Ahmad and Marashdeh 2014; Al-Harahsheh et al. 2014).

A comparison between raw volcanic tuff and synthesized geopolymer is illustrated in Fig. 1. Upon reaction, the peak of the major mineral (phillipsite) in the raw material (tuff) disappeared in the XRD

Table 3 The chemical composition for raw volcanic tuff and geopolymer

Compound (%)	Raw volcanic tuff % mass	Geopolymer % mass
SiO_2	44.56	35.87
Al_2O_3	11.74	9.6
Fe_2O_3	10.78	9.22
CaO	10.46	10.5
MgO	8.81	7.76
K_2O	1.5	1.23
P_2O_5	0.52	0.39
TiO_2	2.63	2.35
Na_2O	1.87	13.55
MnO	0.11	0.11
L.O.I.	7.1	8.7

patterns of volcanic tuff-based geopolymer due to dissolution process (Rushdi et al. 2009). During the geopolyemerization process, the sodium ions substitute Ca and Mg ions in their aluminosilicates and silicates expedite the dissolution of these species (El-Eswed et al. 2012) and subsequently reduce the concentration of phillipsite and diopside in the synthesized structure.

Chapazite and diopside also disappeared during geopolymerization, whereas sodalite appeared clearly. Rushdi et al. (2009) reported that a solid and stable material with hydroxysodalite (sodalite), zeolite, and feldspatiod (sodalite) was formed because of the geopolymerization reaction. Dimitrios et al. (2007) also found that hydroxysodalite, Na8(AlSiO4)6(OH)4, was formed as the concentration of NaOH increased from 4.47 to 10.25. An increase in the dissolution of Si and Al resulted in a new amorphous aluminosilicate phase in the geopolymeric samples. Krol et al. (2014) found that in strong alkaline condition (5.0 M NaOH) and elevated temperature (90 °C), zeolite completely disappeared after 6 h at the same time sodalite crystals appeared. It was suggested that at higher temperatures and NaOH concentrations, zeolite is unstable and transforms into sodalite (Krol et al. 2014). Hydroxysodalite, which ranges from amorphous to microcrystalline material, consists of SiO_4 and AlO_4 tetrahedral linked alternately by sharing all the oxygen atoms. It has six member rings with aperture diameter of 0.22 nm, which is smaller than zeolite pore size. The cations such as Ag^{2+}, Cu^{2+}, and Cs^+ can be exchanged with sodalite cage cation (β-cages) which explains the efficiency of sodalite in removing heavy metals (Mon et al. 2005).

3.1.2 The XRF Characterization

The chemical composition of volcanic tuff samples and the synthesized geopolymer obtained by XRF technique are presented in Table 3. The results obtained showed clearly that the amount of SiO_2 and Al_2O_3 decreased significantly after geopolymerization from 44.56 to 35.87 % and from 11.74 to 9.60 %, respectively. This decrease is due to the increase in Na_2O and water content (Wu et al. 2008) where sodium and hydroxyl group incorporated within the structure of the geopolymer during the geopolymerization process.

According to results presented in Table 3, the ratio of SiO_2/Al_2O_3 for volcanic tuff sample was 3.79 wt/wt, which falls within the suitable range reported for
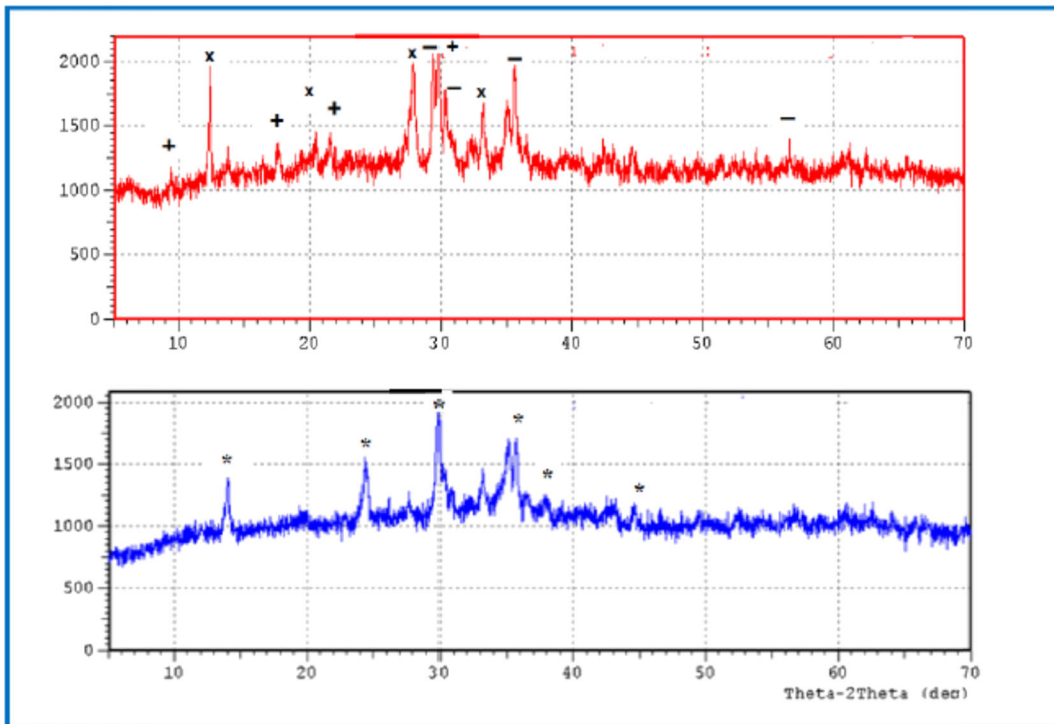
Fig. 1 XRD patterns for volcanic tuff (*top*) and volcanic tuff-based geopolymer (*down*), where *plus sign* is chapazite, *multiplication sign* is philipsite, *en-dash* is deposite, and *asterisk* is sodalite

geopolymer formation (3.3 and 6.5) (Van Jaarsveld et al. 1997).

The high calcium content in the current volcanic tuff sample (10.46 %) may have adverse impact on the geopolymerization process. It has been reported that if CaO is present at levels above 3 % by mass, it interferes with crystallization during the synthesis of geopolymer (Provis 2006). The negative impact of CaO can be attributed to the rapid dissolution of calcium by NaOH solutions, which results in precipitation of $Ca(OH)_2$, which will lower the pH and subsequently affects the rate of geopolymerization. High amount of Fe_2O_3 (10.78 %) has similar effects as CaO (Provis 2006).

3.1.3 The SEM Observations

The SEM showed that the volcanic tuff particle had mostly spherical shapes, whereas other particles had cubic, elongated, and irregular shapes (Fig. 2). After geopolymerization, some of the tuff particles appeared with different shapes, which may indicate incomplete dissolution of raw materials. SEM also showed a highly

Fig. 2 SEM for volcanic tuff (*left*) and geopolymer (*right*)
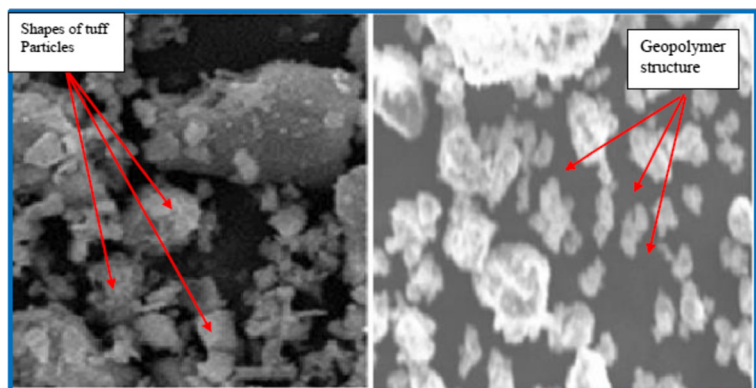
porous appearance of geopolymer in comparison with natural volcanic tuff, indicating the formation of new cavities in the geopolymer structure. Natural volcanic tuff is considered a porous material, although the activation process created additional cavities, which provided appropriate diffusion channels for metal ions into the interior of the geopolymer and subsequently enhanced the adsorption of metals inside these pores (Khalili Fawwaz et al. 2013).

3.1.4 FTIR Spectra

Figure 3 shows the main FTIR absorption bands of volcanic tuff and the synthesized geopolymers. The FTIR spectrum of volcanic tuff samples showed asymmetric stretching vibrations of Si–O–Al band that appeared at about 1035 cm^{-1}, whereas for geopolymer samples, the stretching became sharper and shifted to a lower frequency (<100 cm^{-1}) indicating the formation of amorphous aluminosilicate gel phase, due to the

dissolution of tuff amorphous phase in NaOH-activating solutions. Panias and Giannopoulou (2006) found similar results where the band appeared at 1085 cm^{-1} and shifted to lower frequencies of 986 cm^{-1} because of geopolymerization. A new peak at about 860 cm^{-1} associated with Si–O–Al and Si–O–Si symmetric stretching was clearly seen after geopolymerization. Same peak was found by Alvarez-Ayuso et al. (2008) at frequencies of 810, 750, and 590 cm^{-1}.

Bands' peak with frequencies of 2430, 1460, and 1270 was found in the spectra of geopolymer samples. These bands are associated with H–O–H stretching and –OH bending, respectively. The presence of these absorption bands indicated weakly bound molecules of water, either adsorbed by the surface or trapped in large cavities (Swanepoel et al. 2002). Other spectra band that appeared at about 1430 cm^{-1} in the geopolymer sample represents carbonate asymmetric stretching of O–C–O. This band could be attributed to the high content
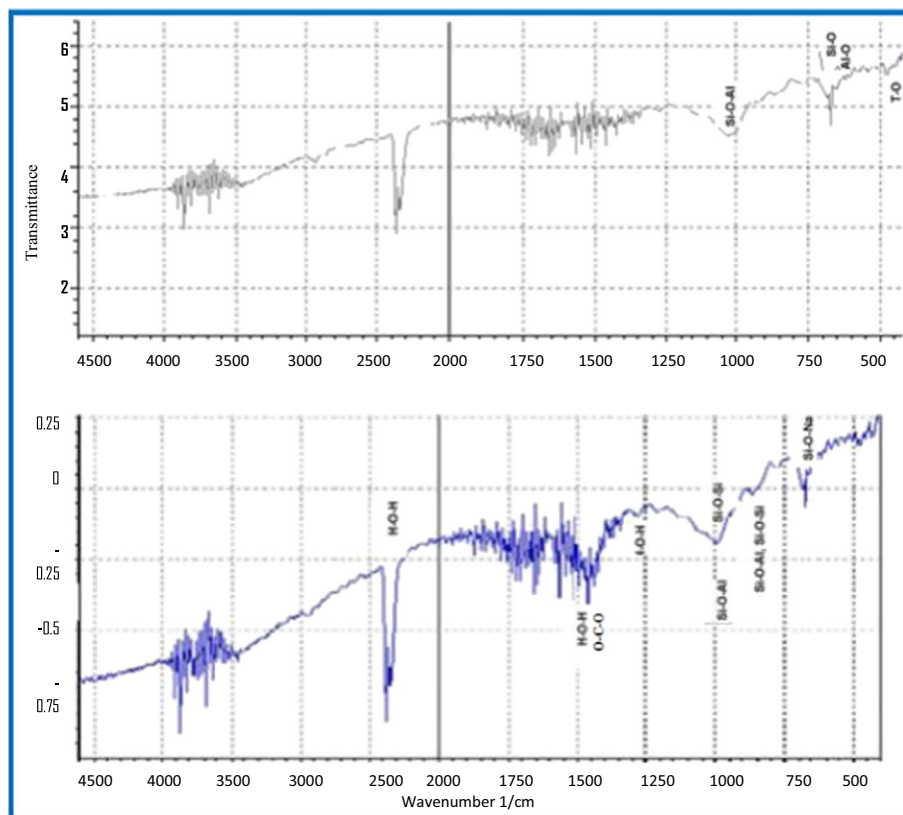

Fig. 3 FTIR spectra of the volcanic tuff (*top*) and geopolymer (*down*)

of calcite in the raw material (Onisei et al. 2012) or due to the presence of sodium carbonate formed through atmospheric carbonation of NaOH (Dimitrios et al. 2007; Onisei et al. 2012). The same band was found by Onisei et al. (2012) at 1445 and Dimitrios et al. (2007) at frequencies of 1430 and 1420 and Alvarez et al. (2008) at the frequency of 1435 cm^{-1}.
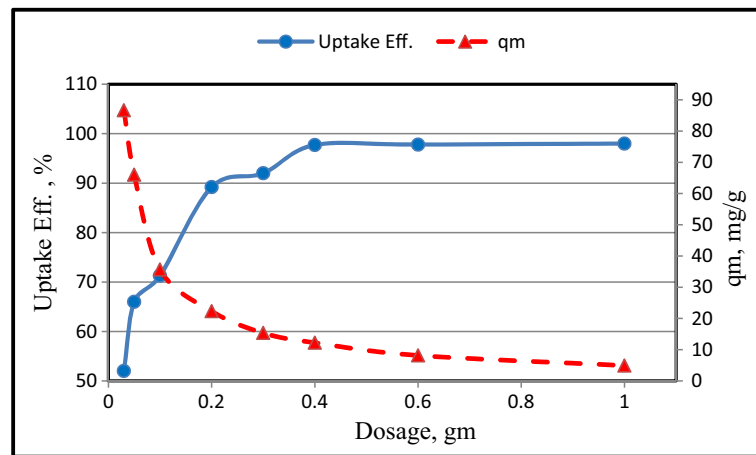
3.2 Uptake Efficiency of Volcanic Tuff and Synthesized Geopolymer

The percentage uptake of Zn^{2+} by natural volcanic tuff and synthesized geopolymer was investigated at pH value of 7 and a dose rate of 0.6 g for solid material, with initial concentration of Zn^{2+} at 100 ppm. It was found that the maximum uptake

Table 4 Comparison of the current study with previous ones

Used materials	Efficiency	q mg/g	References
Activated fruit of *Kigelia pinnata*	84 %	–	Shobana et al. (2014)
Pulp waste	60 %	2.2	Sampranpiboon et al. (2014)
Bentonite	64	54*	Kaya and Oren (2005)
Activated carbon prepared from almond husks	92 %	4.5	Hasar et al. (2003)
Kaolin	94 %	12.23	Meroufel et al. (2013)
Phosphogypsum	–	9.3	Chafik et al. (2014)
Fly ash	100	0.11	Agarwal et al. (2012)
Gyrolite	72 %	–	Baltakys et al. (2012)
Walnut and poplar leaves	82 %	–	Salim et al. (2003)
Sago waste	74 %	10.4	Wahi et al. (2010)
Rice husk	–	101.01	Dada et al. (2012)
Streptomyces rimosus biomass	–	29.6	Chergui et al. (2007)
*Penicillium simplicissim*um	–	250	Fan et al. (2008)
Papaya wood	66.8 %	–	Saeed et al. (2005)
Aspergillus niger	–	23.70	Yun-Guo et al. (2006)
Bentonite		20.5	Ghomri et al. (2013)
Mucor rouxii biomass	–	1.36	Yan and Viraraghavan (2003)
Activated carbon prepared from Van apple pulp	–	11.72	Depci et al. (2012)
Activated carbon	–	11.24	Mishra and Patel (2009)
Kaolinite	–	3.05	Mishra and Patel (2009)
Bentonite	–	9.12	Mishra and Patel (2009)
Penicillium chrysogenum	–	11.11	Puranik and Paknikar (1999)
Tannic acid immobilized	–	1.23	Meroufel et al. (2013)
Carbon aerogel	–	1.183	Meroufel et al. (2013)
Sugar beat	–	0.176	Meroufel et al. (2013)
Fly ash	–	11.11	Meroufel et al. (2013)
Activated alumina	–	13.69	Meroufel et al. (2013)
Clarified sludge	–	5.53	Meroufel et al. (2013)
Humic acid	–	6.12	Meroufel et al. (2013)
Granite	–	8.64	Meroufel et al. (2013)
Saw dust	–	2.58	Meroufel et al. (2013)
Current work	97 %	14.7	

Fig. 4 Effect of geopolymer dosage on the adsorption of Zn

efficiency of volcanic tuff was 78.51 % as against 97.78 % for geopolymer, and the uptake capacity was 6.54 and 8.15 mg/g, respectively. This result indicated that the geopolymerization process succeeded in producing additional pores, which improved its capacity for Zn^{2+} uptake. The increase in the removal efficiency (19.27 %) buttressed the significance and feasibility of producing geopolymer from natural volcanic tuff.

Comparison of the results obtained with previous studies (Table 4) indicated a high uptake of geopolymer-based volcanic tuff in Zn^{2+} removal, which is more than most of the other materials used such as activated carbon (Depci et al. 2012), kaolinite (Mishra and Patel 2009), bentonite (Mishra and Patel 2009), sugarbeet (Meroufel et al. 2013), and fly ash (Agarwal et al. 2014). Few other materials provided higher uptake capacity

such as clarified sludge (Meroufel et al. 2013), rice husk (Dada et al. 2012), and *Streptomyces rimosus* biomass (Chergui et al. 2007).

3.3 Effect of Geopolymer Dosage

The effect of different geopolymer dosages (0.03–1 g) on the adsorption of Zn^{2+} was studied under constant conditions (pH = 7, C_0 = 100 ppm, T = 25 °C). The result obtained indicated that the uptake efficiency increased significantly from 52.33 to 97.7 % as the geopolymer dose increased from 0.03 to 0.4 g, whereas a slight increase was observed at a dose of 1 g (98.05 %). Adsorption capacity decreased from 86.70 to 12.21 and 4.9 mg/g as the dose increased from 0.03 to 0.4 and 1 g, respectively (Fig. 4). The higher dose usually provides the higher removal efficiency while the uptake capacity (mg/g) decreases accordingly. Higher dose of

Fig. 5 Effect of contact time on the adsorption of Zn
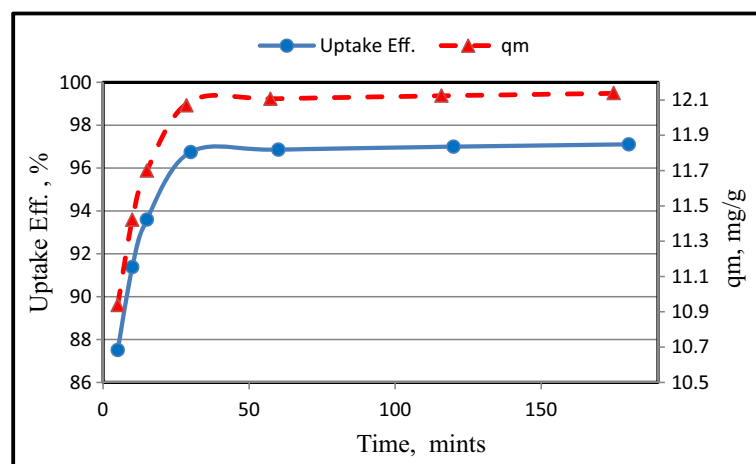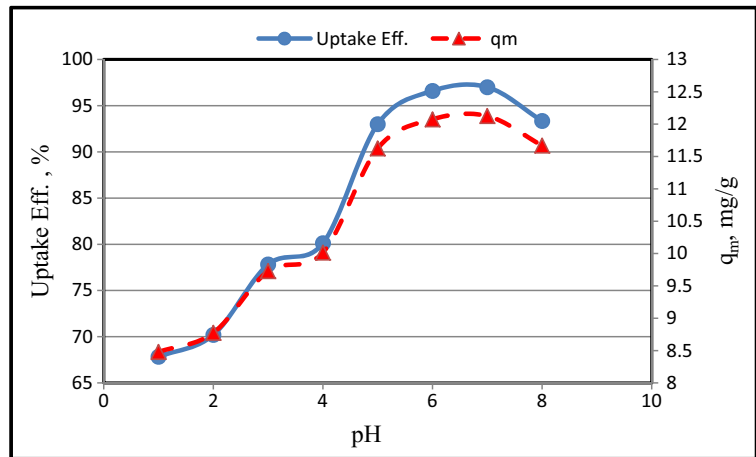
Fig. 6 Effect of pH value on the adsorption of Zn

geopolymer resulted in an increase in the available surface area and pores of geopolymer samples, which increased the available sites for binding of Zn ion and thereby enhances the adsorption from solution to geopolymer (Donat et al. 2005 and Depci et al. 2012). Agarwal et al. (2014) found that Zn uptake efficiency increased from 45.8 to 76.1 % and 100 % as the adsorbent (coal fly ash) dose increased from 1 to 10 and 18 g, respectively.

3.4 Effect of Contact Time

The time dependence behavior of Zn ion was investigated by varying the contact time between the adsorbate (Zn) and adsorbent (geopolymer) in the range of 5–180 min under optimum conditions of the other parameters.

Figure 5 shows that the adsorption of Zn ion by geopolymer increased sharply as the time increases up to 30 min, after which it increased slightly during the studied period (3 h). At an equilibrium time of 30 and 120 min, the uptake percent was 96.75 and 97.0 % with uptake capacity of 12.09 and 12.13 mg/g, respectively. Such increase in the removal efficiency between 30 and 120 min is very low (0.25 %); therefore, a 30-min contact time is considered a feasible time for adsorption. It was found that a contact time of 60 min was sufficient for Zn^{2+} removal by activated fruit of *Kigelia pinnata* (Shobana et al. 2014) and by activated carbon prepared from almond husks (Hasar et al. 2003). Other researchers reported shorter contact time (Saeed et al. 2005; Wahi et al. 2010; Baltakys et al. 2012) and longer contact times (Agarwal et al. 2014; Wasewar et al. 2008; Sampranpiboon et al. 2014). Although the contact time is very important, however, the uptake efficiency at a certain time depends on the characteristics of adsorbent, temperature, adsorption doses, and other control conditions.

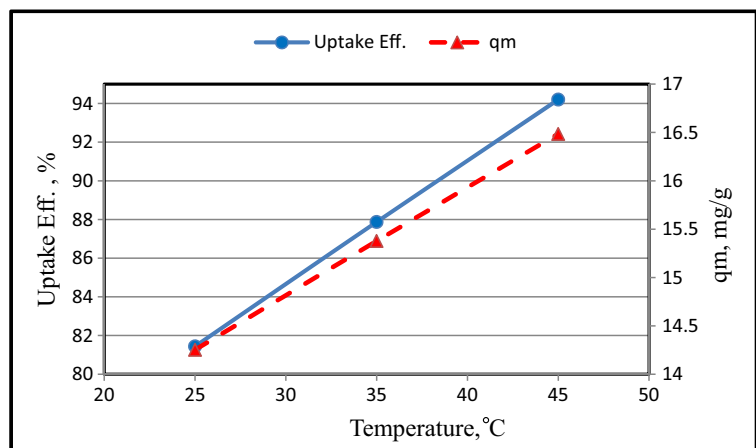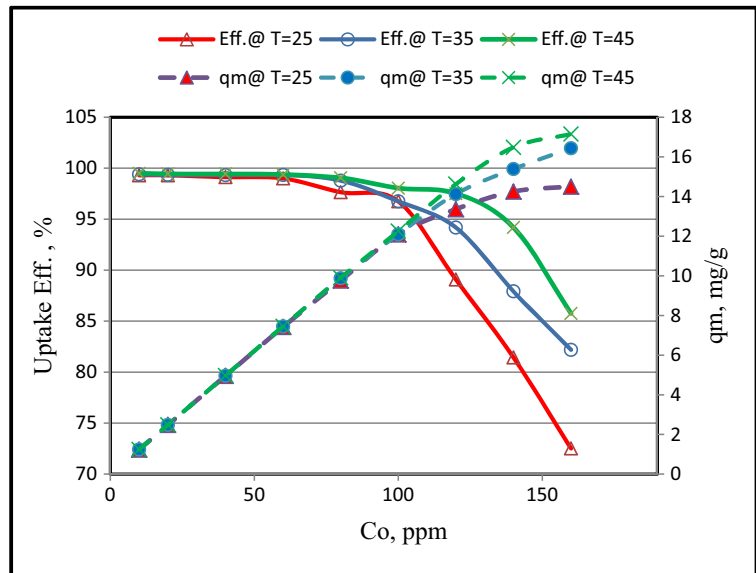**Fig. 7** Effect of temperature on Zn adsorption at $C_0 = 140$ ppm

Fig. 8 Effect of temperature on Zn adsorption at different C_0

3.5 Effect of pH Value on the Adsorption of Zn^{2+}

The effect of pH on Zn^{2+} adsorption was investigated under batch procedure with pH range between 1.0 and 8. The results obtained indicated that the adsorption efficiency increased from 67.83 to 97 % as pH increased from 1 to 7, while it decreased slightly to 93.35 % at pH 8 (Fig. 6). This indicates that the zero point of charge is at pH 7.0. As the reaction progresses with an increase in pH, the surface of the synthesized geopolymer becomes negatively charged, and electrostatic repulsion decreases with rising pH due to reduction of positive charge density on the sorption edges resulting in an

increase in metal adsorption (Meroufel et al. 2013). Since there is no sharp increase in uptake values at high pH values, it indicates that no precipitation occurred within the studied pH ranges. At a pH range between 4.00 and 7.00, Zn ion exchanged with the exchangeable cations present at the geopolymer sites resulted in significant reduction in Zn ion concentration. At higher pH values, zinc hydroxyl species was involved in either the adsorption or precipitation onto the adsorbent, which adversely affected the uptake efficiency (Kaya and Oren 2005). Agarwal et al. (2014 and Bayat 2002) achieved high Zn^{2+} removal at a pH of 7. Others reported lower pH values ranging from 4.2 to 6.9 (Shobana

Fig. 9 Effect of initial concentration on Zn adsorption at $T = 25$ °C and pH = 7

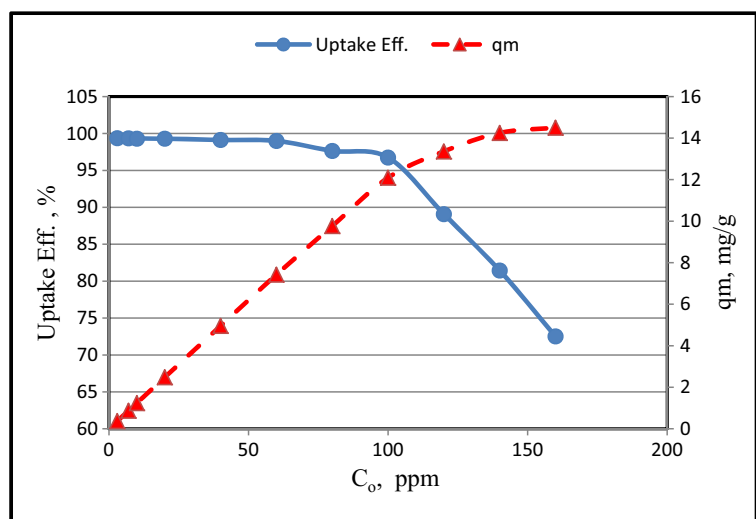**Table 5** Results of Langmuir models

Model	pH = 5			pH = 6			pH = 7		
	R^2	q_m	K	R^2	q_m	K	R^2	q_m	K
Langmuir 1	0.999	14.83	0.70	0.999	14.79	0.91	0.999	14.70	1.26
Langmuir 2	0.998	13.20	1.14	0.998	13.62	1.44	0.999	15.52	1.28
Langmuir 3	0.974	13.70	1.06	0.962	13.64	1.43	0.978	14.42	1.47
Langmuir 4	0.973	13.86	1.04	0.962	13.82	1.39	0.978	14.54	1.44

et al. 2014; Saeed et al. 2005; Ghomri et al. 2013; Salim et al. 2003; Wasewar et al. 2009) and higher pH values (Wahi et al. 2010). It is worth mentioning that the optimum pH value for metal removal depends on many conditions but not limited to the type of adsorbent, adsorption mechanism, and the activation process.

3.6 Effect of Temperature on Zn^{2+}

Figure 7 shows the effect of temperature on Zn^{2+} adsorption, where the uptake efficiency increased linearly with an increase in temperature. At low concentration (<100 ppm), the effect of temperature on the removal efficiency was insignificant, whereas the effect is clear at higher concentration (Fig. 8). This behavior can be attributed to the availability of pores. At low concentration, the pores are sufficient to host most of the ions, while at higher concentration, the pores become insufficient and there is a need for additional pores, which could be created by the impact of high temperature. In

addition, at high temperature, an increase in water vaporization results in the formation of micro-cavities and subsequently causes an increase in the uptake capacity (Andini et al. 2008). At 140 ppm, the uptake efficiency increased from 81.44 to 94.2 % with an increase in temperature from 25 to 45 °C, while at lower initial concentration (100 ppm), the uptake efficiency increased from 96.75 to 98.05 %, which indicated an endothermic process. The uptake capacity at 140 ppm also increased from 14.253 to 16.485 mg/g at the same range of temperature.

3.7 Effect of Initial Concentration

Different initial concentrations of Zn^{2+} ranging from 10 to 160 ppm were used to investigate its impact on the adsorption process. Figure 9 shows that the adsorption efficiency decreased from 96.75 % at 100 mg/L to 72.51 % at 160 mg/L, while the uptake capacity increased from 12.09 to 14.50 mg/g for the same range

Fig. 10 Validity of four Langmuir models for Zn adsorption (pH = 7, $T = 25$, q_{exp} = experimental q, q_{cal} = calculated q)
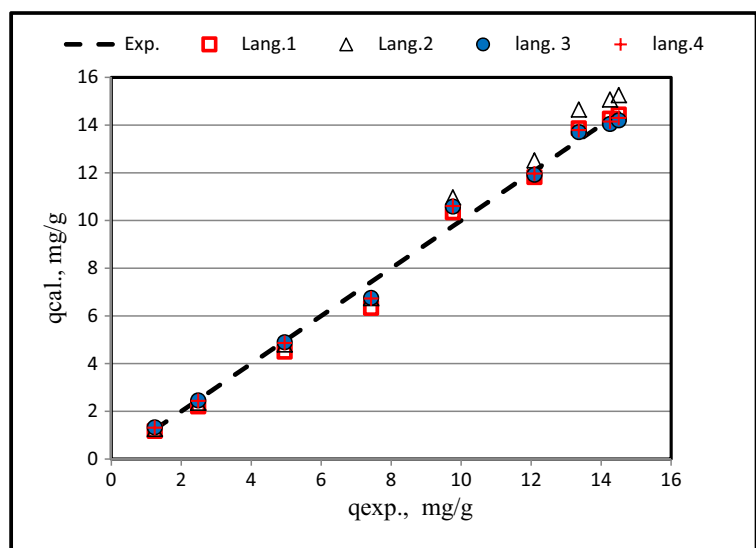
Table 6 Results of Freundlich model

Model	Temperature (°C)	pH = 5			pH = 6			pH = 7		
		R^2	K_f	n	R^2	K_f	n	R^2	K_f	n
Freundlich	25	0.9	4.85	2.68	0.89	5.22	2.82	0.83	5.68	2.91
	35	0.91	4.91	2.56	0.91	5.29	2.73	0.85	5.80	2.78
	45	0.92	5.36	2.55	0.91	5.36	2.67	0.87	5.87	2.71

of concentrations. . Between initial concentrations of 3 and 100 ppm, the removal efficiency decreased slightly from 99.36 to 96.75 % followed by a sharp decrease. As the concentration of the metal increases, the available pores of adsorbent became insufficient to absorb all ions, while the excess ions remained soluble in the solution with no more ions to be adsorbed which explain the stability of the uptake capacity (q) after a certain concentration. Similar result was reported by Agarwal et al. (2014), where the removal efficiency of Zn^{2+} decreased from 100 to 41.8 % and 26.8 % as the initial concentration increased from 5 to 100 and 200 mg/l, respectively.

3.8 Isotherm Study

3.8.1 Langmuir Models

Table 5 illustrates the results of R^2, q_m, and K values for four Langmuir models. It is clear that the coefficients of correlation (R^2) of Langmuir types 1 and 2 were always

more than 0.99 for all pH and temperature values, whereas less fitness was achieved by types 3 and 4 (Fig. 10). According to R^2, the models can be ranked in the order of type 1 > type 2 > type 4 > type 3. In most of cases, types 3 and 4 have the same value of R^2. For all models, the q_m values increased with an increase in temperature which indicated an endothermic adsorption process. At optimum pH value (7), and by using Langmuir type 1 model, the maximum uptake capacity (q_m) increased by 19.9 % from 14.7 to 17.63 mg/g as the temperature increased from 25 to 45 °C. A high KL value (>0.7) indicated a high adsorption affinity of Zn^{2+} on the geopolymer structure (Sampranpiboon et al. 2014). The fitness of Langmuir isotherm for the adsorption process indicated that the adsorption is homogenous and no interaction occurred between the adsorbed species (Al-Jariri and Khalili 2010). Many researchers proved the high validity of Langmuir isotherm model for absorption process (Hasar et al. 2003; Sampranpiboon et al. 2014, Meroufel et al., 2014, Agarwal et al. 2014; Kazmi et al. 2012). The

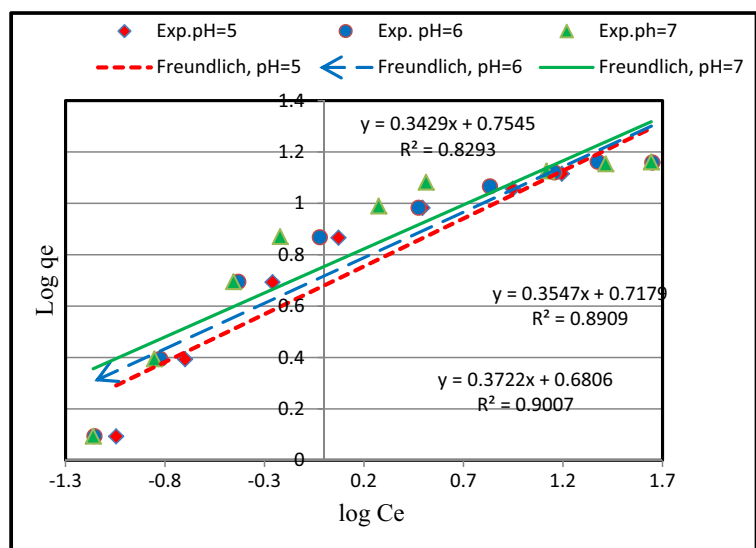**Fig. 11** Validity of Freundlich model for Zn adsorption

Table 7 Results of Redlich-Peterson model ($T = 25$)

Coefficient	pH = 5	pH = 6	pH = 7
R^2	0.99	0.99	0.99
K_{arp}	14.38	16.76	22.29
a_{rp}	1.19	1.29	1.670001
β	0.994	0.964	0.973

dimensionless separation factor (RL) was calculated from the best fit model (Langmuir type 1) at pH of 7, using the following equation (Dada et al. 2012):

$$RL = \frac{1}{1 + KC_0} \tag{11}$$

where K is the Langmuir adsorption constant and C_0 is the maximum initial concentration.

The calculated values for RL were 0.0049, 0.0045, and 0.0034 at temperatures of 25, 35, and 45 °C, respectively. For all temperatures, the values of $0 < RL < 1$ indicated a highly favorable adsorption process (Dada et al. 2012). The values of RL are close to zero, which indicates that the adsorption process is irreversible.

3.8.2 Freundlich Model

The values of n and KF Freundlich parameters were calculated from the intercept and slopes of the corresponding linear plots of Zn^{2+} adsorption onto geopolymer at different temperatures (25, 35, 45 °C) and pH values (5, 6, 7). The values of these parameters with their correlation coefficients (R^2) are given in Table 6.

The correlation coefficient obtained for Freundlich models ranged from 0.83 at pH = 7 and $T = 25$ °C to 0.92 at pH = 5 and $T = 45$ °C as shown in Fig. 11. In comparison with Langmuir models, Freundlich model produced less fitness with adsorption data, which indicates that the homogenous adsorption is better at describing the process compared to heterogeneous adsorption. The n values decreased with an increase in temperature and ranged from 2.55 to 2.91, which indicated a favorable adsorption of Zn^{2+} on geopolymer surface (Tahir and Naseem 2007). Freundlich adsorption constant K_f increased with an increase in temperature and pH and ranged from 4.85 at pH = 5 and $T = 25$ °C to 5.87 at pH = 7 and $T = 45$ °C indicating a high adsorption intensity at higher temperatures (Donat et al. 2005).

3.8.3 Radlich-Peterson Isotherm

It is a hybrid form of Langmuir and Freundlich equations incorporating a linear relation in the numerator and an exponential function in the denominator (Kazmi et al. 2012) and therefore can be applied in either homogenous or heterogeneous systems due to its high versatility.

The values of K_{rp}, a_{rp}, and β were determined by Excel Solver with minimum error calculation (Table 7). The coefficient of correlation values were >0.99 for all pH and temperature ranges, which indicates a high fitness of the model with adsorption process (Figs. 12 and 13). Since the value of β is close to 1, this indicates that the adsorption system is homogenous which supported Langmuir assumption

Fig. 12 Validity of Radlich-Peterson isotherm model at different pH ($T = 25$)
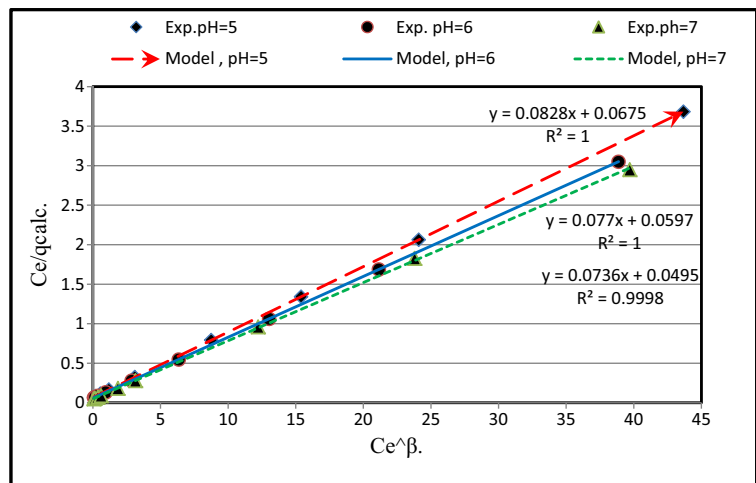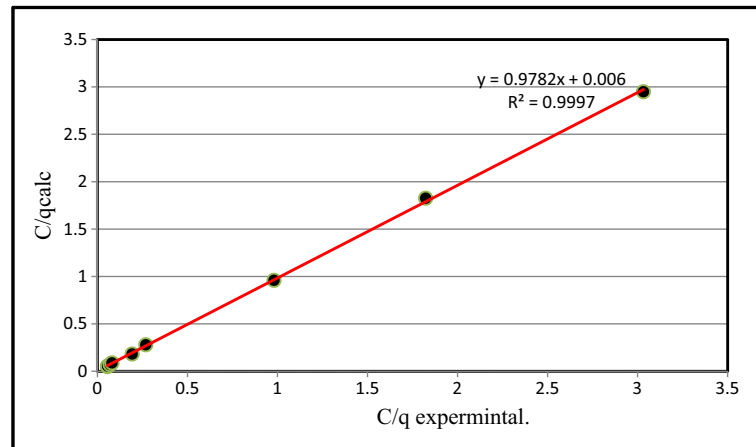
Fig. 13 Experimental and calculated C/q according of Radlich-Peterson model (pH = 7, $T = 25$)

(Kazmi et al. 2012). Previously, Radlich-Peterson model showed excellent fitting for the experimental data of Zn^{2+} removal by pulp waste (Sampranpiboon et al. 2014), by kaolinite (Shahmohammadi-Kalalagh and Babazadeh 2014), and by palm tree trunk (Abuh et al. 2013).

3.9 Calculation of Errors

Two measures (MSE and χ^2) were used to determine the error of the predicted values of C_e/q for Langmuir type 1, Freundlich, and Radlich-Peterson models. Table 8 shows that Radlich-Peterson model has the lowest MSE and χ^2 values followed by Langmuir type 1, while Freundlich model has the highest error values. This result buttressed the validity of Radlich-Peterson and Langmuir models for the adsorption process. Although both models have almost the same R^2, there was a significant difference in MSE and χ^2 values between the two models, which indicates that R^2 could be used for trend purpose only, and the two equal values of R^2 do not necessarily mean equal errors.
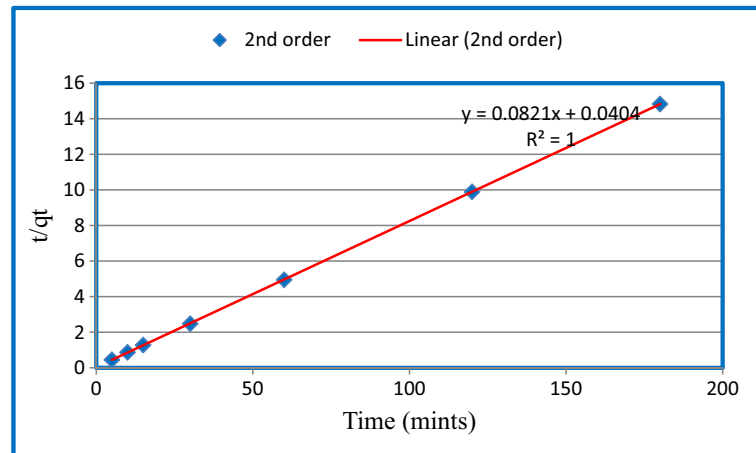
3.10 Kinetic of Adsorption

The results obtained indicated that the pseudo-second-order model shows the best fitness of the experimental data followed by the pseudo-first-order, while the intraparticle diffusion model had the lowest fitness with R^2 values of 1, 0.89, and 0.6, respectively (Fig. 14). In addition, the second-order model showed the best fitness in estimation of q_e as shown in Fig. 15. Many researches substantiated the validity of the pseudo-second-order model for the kinetics of Zn^{2+} adsorption (Fan et al. 2008; Ozdemir et al. 2004; Yun-Guo et al. 2006, Ghomri et al. 2013). The linear plot of intraparticle model (q_e against $t^{0.5}$) did not pass through the origin, which indicates the existence of some boundary layer effect (Arivoli et al. 2013).

3.11 Thermodynamic Study

The calculated values for thermodynamic parameters are given in Table 9. It was found that the distribution coefficients (K_d) increased with an increase in temperature and pH. Higher K_d values indicated that higher amounts of Zn^{2+} had been retained by the adsorbent

Table 8 Results of models error calculation for c/q at $T = 25$ °C

Model	pH = 5			pH = 6			pH = 7		
	R^2	MSE	χ^2	R^2	MSE	χ^2	R^2	MSE	χ^2
Langmuir 1	0.99	0.002	0.034	0.99	0.001	0.009	0.99	0.0003	0.016
Freundlich	0.9	0.104	0.503	0.89	0.098	0.551	0.83	0.1116	0.586
Redlich-Peterson	0.99	0.001	0.010	0.99	0.001	0.013	0.99	0.0001	0.003

Fig. 14 Relationship of t/q with time according to the pseudo-second-order model

The values of ΔH_o and ΔS_o ranged from 20.48 to 32.63 and from 0.116 to 0.158 kJ/mol, respectively, and both increased with an increase in temperature and pH. ΔH values were more than $T\Delta S$, which means that the adsorption process was mostly entropy-controlled (Sismanoglu et al. 2004). A positive value of ΔH_o indicates that adsorption is an endothermic process in which the energy of dehydration exceeds the exothermicity of the metal ions bonded to the geopolymer surface (Ghomri et al. 2013; Al-Jariri and Khalili 2010; Meroufel et al. 2013). Since ΔH_o value is less than the value reported for heat of chemisorption (80–200 kJ/mol) (Saha and Chowdhury 2015), it can be ensured that the uptake of Zn^{2+} by the geopolymer surface is a physiosorption process.

and removed from the solution (Ramachandran and D'Souza 2013).

The positive values of ΔS_o indicate that the entropy of the system increases after the adsorption process which also supports the result of endothermicity and the stability of the adsorption (Al-zboon et al. 2011). When the metal ions penetrate the geopolymer matrix, the water molecules that were previously united with the ions will be released and dispersed in the solution that enhances the disturbance of the heterogeneous system, which explain the increase of entropy with increase in temperature (Donat et al. 2005; Al-zboon et al. 2011). The small values of ΔS_o indicate that the adsorption process has little affinity for the heterogeneous system. Fan et. al. (2008) reported that the adsorption of Zn^{2+} by *Penicillium simplicissimum* was endothermic and spontaneous in nature. Also, Ghomri et al. (2013) found an endothermic adsorption process of Zn^{2+} by bentonite. The ΔG values ranged from −19.21 to
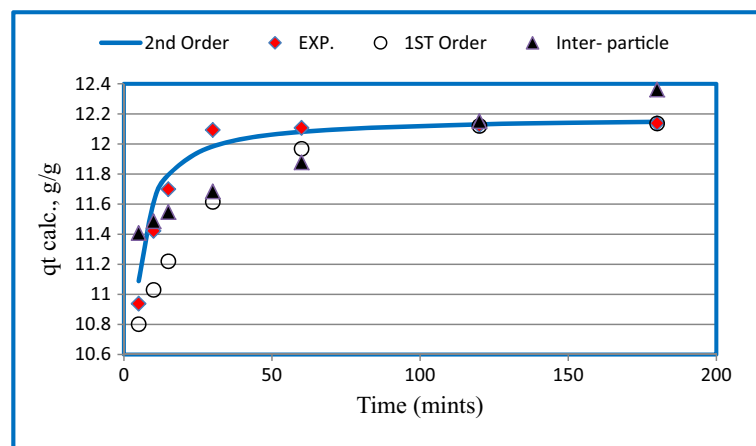
Fig. 15 Fitness of the models to the q_t experimental data

Table 9 The calculated thermodynamic parameters

T (Kelvin)	pH = 5				pH = 6				pH = 7			
	R^2	ΔH_o	ΔS_o	ΔG	R^2	ΔH_o	ΔS_o	ΔG	R^2	ΔH_o	ΔS_o	ΔG
298	1	20.48	0.116	−14.32	0.963	23.47	0.127	−14.4	0.967	32.63	0.158	−14.47
308				−16.65				−16.94				−17.63
318				−17.82				−18.21				−19.21

−14.32 kJ/mol and decreased with an increase in temperature at rates of −0.17, −0.19, and −0.23 kJ/ mol 1 °C for pH of 5, 6, and 7, respectively, as shown in Fig. 16. The higher change in ΔG was found at pH = 7 (−0.23 kJ/mol 1 °C) which indicates the favorability of adsorption at higher pH.

The negative ΔG values at different temperatures buttressed the mentioned characteristics of the adsorption process, which are endothermic, spontaneous, and physiosorption nature (Sharmaa et al. 2014). Since Zn^{2+} uptake happened effectively at both low and high temperature, it can be inferred that both adsorption and ion exchange mechanism occurred (Ghomri et al. 2013). Wasewar et al. (2009) used tea factory waste for Zn^{2+} removal and found that the adsorption process was endothermic with ΔH, ΔS, and ΔG values of 11.55, 31.24, and −0.0095 kJ/mol, respectively.

3.12 Activation Energy and Sticking Probability

In adsorption, the activation energy is defined as the energy that the ion must overcome for it to react or interact with the adsorbent surface (Saha and Chowdhury 2015). There is a direct relationship between the removal efficiency, the activation energy (E_a), and the sticking probability (S^*) as shown in Eqs. 12, 13, and 14 below (Ayawei et al. 2015):

$$\theta = 1 - \frac{C_e}{C_0} \tag{12}$$

$$S^* = (1-\theta)e^{\frac{E_a}{RT}} \tag{13}$$

Which can be linearized as follows:

$$\text{Ln}(1-\theta) = S^* - \frac{E_a}{RT} \tag{14}$$

The values of E_a and S^* can be calculated from the slope and intercept of the plot of $\ln(1-\theta)$ *against* $1/T$, respectively. The E_a and the S^* were calculated for the experimental data in order to support the claim that physical adsorption is the predominant mechanism. The positive value calculated for E_a (23.41 kJ/mol) indicated the endothermic nature of the adsorption process, which conforms to previous results obtained.

It can be concluded that the adsorption process of Zn^{2+} by the geopolymer surface is a simple physical adsorption process, because the values of activation

Fig. 16 $\Delta G°$ at different T and pH
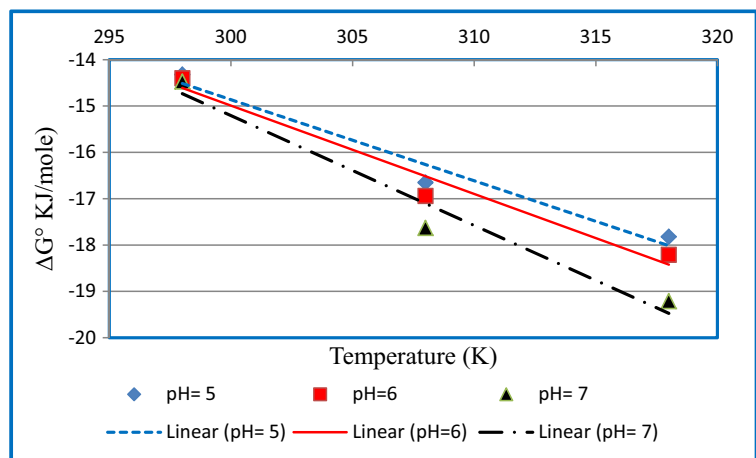
energy (23.41) were in the range of 21 to 42 kJ/mol (Sismanoglu et al. 2004). The calculated $S*$ value was very low (3×10^{-6}) indicating a high stick of the ions to the geopolymer surface ($S* \ll 1$) (Kumar et al. 2014).

4 Conclusion

This study examined the suitability of natural volcanic tuff for geopolymer production and the removal of Zn^{2+}. The study includes the characterization of volcanic tuff and geopolymer. The parameters, which could have an effect on the adsorption process, were investigated. Isotherm and kinetic studies were also carried out.

It was found that the maximum uptake efficiency of geopolymer was 97.78 % against 78.51 % for volcanic tuff, and the uptake capacity (at pH = 7 and dosage of 0.7 g) was 8.15 and 6.54 mg/g, respectively, which indicated the feasibility of producing geopolymer form natural volcanic tuff.

The best pH for Zn^{2+} removal was = 7, and the feasible mixing time = 30 min. The removal efficiency increased with geopolymer dosage increase, contact time increases, temperature increases, and initial concentration decreases.

The isotherm study showed best fit on Langmuir and Radlich-Peterson models, while Freundlich model has the highest error values. The maximum uptake capacity obtained from Langmuir model increased from 14.7 to 17.63 mg/g as the temperature increased from 25 to 45 °C. The pseudo-second-order model showed the best fitness for the experimental data followed by pseudo-first-order model.

Based on the results, it can be concluded that natural volcanic tuff could be used successfully as a base of geopolymer for Zn^{2+} removal with high efficiency up to 97.7 % and an uptake capacity of 14.7 mg/g at 25 °C. The adsorption process is endothermic, spontaneous, and irreversible with high sticking of ions to the geopolymer surface.

References

Abdul Kadir, A., Abdullah, A., & Wai, L. K. (2013). Study on ferum (Fe) and zinc (Zn) removal by using rice bran at Sungai Pelepah, Kota Tinggi, Johor. *Advances in Environmental Biology, 7*(12), 3580–3586.

Abdul Rahim, R. H., Rahmiati, T., Azizli, K. A., Man, Z., Nuruddin, M. F., & Ismail, L. (2014). Comparison of using NaOH and KOH activated fly ash-based geopolymer on the mechanical properties. *Materials Science Forum, 803*, 179–184.

Abuh, M. A., Akpomie, G. K., Nwagbara, N. K., & Nwafor, E. C. (2013). Equilibrium isotherm studies for the biosorption of Cu (II) and Zn (II) from aqueous solution by unmodified lignocellulosic fibrous layer of palm tree trunk—single component system. *International Journal of Engineering Science Invention, 2*(6), 27–35.

Agarwal, A. K., Mahendra, S., Kadu, C, Pandhurnekar, P., & Muthreja I. L. (2014). Langmuir, Freundlich and BET adsorption, isotherm studies for zinc ions onto coal fly ash. *International Journal of Application or Innovation in Engineering & Management 3*(Issue 1).

Agarwal, A. K., Kadu, M. S., Pandhurnekar, C. P., & Muthreja, I. L. (2012). Kinetics and adsorption isotherm study of removal of Zn+2 ions from aqueous solution using thermal power plant fly ash. *International Journal of Environmental Science and Development, 3*(4), 376–381.

Ahmaruzzaman, M. (2010). A review on the utilization of fly ash. *Progress in Energy and Combustion Science, 36*(3), 327–363.

Al Bakri, A. M., Mustafa, H., Kamarudin, M., Bnhussain, I., Khairul Nizar, A., Rafiza, R., & Zarina, Y. (2012). The processing, characterization, and properties of fly ash based geopolymer concrete. *Review of Advance Science, 30*(2012), 90–97.

Al-Harahsheh, M. S., Shawabkeh, R., Batiha, M., Al-Harahsheh, A., & Al-Zboon, K. (2014). Sulfur dioxide removal using natural zeolitic tuff. *Fuel Processing Technology, 126*, 249–258.

Al-Harahsheh, M. S., Zboon, K. A., Al-Makhadmeh, L., Hararah, M., & Mahasneh, M. (2015). Fly ash based geopolymer for heavy metal removal: a case study on copper removal. *Journal of Environmental Chemical Engineering, 3*(3), 1669–1677.

Ali, A. A. & El-Bishtawi, R. (1997) Removal of lead and nickel ions using zeolite tuff. *Journal of Chemical Technology and Biotechnology 69*, (No. 1), 27–34.

Ali Ahmad, M. A.-H., & Marashdeh, L. M. (2014). Removal of aqueous chromium (III) ions using Jordanian natural zeolite tuff in batch and fixed bed modes. *Jordan Journal of Earth and Environmental Sciences, 6*(2), 45–51.

Al-Jariri, J. S., & Khalili, F. (2010). Adsorption of Zn(II), Pb(II), Cr(III) and Mn(II) from water by Jordanian bentonite. *Desalination & Water Treatment, 21*(1–3), 308–322.

Almjadleh, M., Alasheh, S., & Raheb, I. (2014). Use of natural and modified Jordanian zeolitic tuff for removal of cadmium(II) from aqueous solutions. *Jordan Journal of Civil Engineering, 8*(3), 332–343.

Al-Shaybe, M., & Khalili, F. (2009). Adsorption of thorium (IV) and uranium (VI) by the Tulul al-Shabba Zeolitic Tuff, Jordan. *Jordan Journal of Earth Environmental Science, 2*(1), 108–119.

Alvarez-Ayuso, E., Querol, X., Plana, F., Alastuey, A., Moreno, N., Izquierdo, M., Font, O., Moreno, T., Diez, S., Vazquez, E., & Barra, M. (2008). Environmental, physical and structural characterization of geopolymer matrixes synthesized from coal (co-combustion fly ashes). *Journal of Hazardous Materials, 154*(1–3), 175–183.

Al-Zboon, K. K., & Al-Zou'by, J. (2015). Effect of volcanic tuff on the characteristics of cement mortar. *European Journal of Environmental and Civil Engineering*. doi:10.1080/19648189.2015.1053151.

Al-zboon, K., Al-Harahsheh, M., & Bani hani, F. (2011). Fly ash based geopolymer for Pb removal from aqueous solution. *Journal of Hazardous Materials, 188*(1–3), 414–421.

Al-Zou'by Jehad, Y., Kamel, K. A-Z, Al-Tabbal, J. A. (2013). Low-cost treatment of grey water and reuse for irrigation of home garden plants. *Environmental Engineering and Management Journal*. http://omicron.ch.tuiasi.ro/EEMJ/pdfs/accepted/242_743_Al-Zboon_12.pdf.

Amenaghawon, N. A., Aisien, F. A., & Agho, O. E. Application of recycled rubber from scrap tyres in the adsorption of toluene from aqueous solution. *Journal of Applied Science Environment Management 17* (3), 411–417.

Andini, S., Cioffi, R., Colangelo, F., Grieco, T., Montagnaro, F., & Santoro, L. (2008). Coal fly ash for the manufacture of geopolymer-based products. *Waste Management, 28*(2), 416–423.

Arivoli, S., Marimuthu, V., & Mohamed Jahangir, A. R. (2013). Equilibrium, kinetic and thermodynamic study on chromium (VI) removal from aqueous solution using strychnos Nux-Vomica L. *Int Journal of Engineering Research and Applications, 3*(6), 1321–133.

Armagan, B., & Toprak, F. (2012). Optimum Isotherm parameters for reactive azo dye onto pitstachio nut shells: comparison of linear and non-linear methods. *Polish Journal of Environmental Studies, 22*(4), 1007–1011.

Astutiningsih S. and Y. Liu, 2005, Geopolymerization of Australian slag with effective dissolution by the alkali. In Geopolymer: green chemistry and sustainable solution, proceeding of Geopolymer congress 2005, edited by Joseph Davidovits, Institute of geopolymer, Paris, pp. 69–73.

Ayawei, N., Inengite, A. K., Wankasi, D., & Dikio, E. D. (2015). Synthesis and sorption studies of lead (II) on Zn/Fe layered double hydroxide. *American Journal of Applied Chemistry, 3*(3), 124–133.

Baltakys, K., Eisinas, A., Barauskas, I., Prichockiene, E., & Zaleckam, E. (2012). Removal of Zn(II), Cu(II) and Cd(II) from aqueous solution using gyrolite. *Journal of Scientific & Industrial Research, 71*(8), 566–572.

Bayat, B. (2002). Combined removal of zinc (II) and cadmium (II) from aqueous solutions by adsorption onto high-calcium Turkish fly ash. *Water, Air, and Soil Pollution, 136*(1–4), 69–92.

Chafik, D., Bchitou, R., & Bouhaouss, A. (2014). The removal of Zinc in an aqueous solution by the phosphogypsum: modeling and optimizing. *Australian Journal of Basic and Applied Sciences, 8*(2), 331–335.

Chaudhary, R., Khale, D., & Badur, S. (2012). Leaching behavior effectiveness of curing days (7 & 28) of solidified/stabilized fly ash based geopolymer of solidified/stabilized fly ash based geopolymer (multi-metal bearing sludge): experimental and modeling study. *Journal of Environment Science & Engineering, 54*(2), 268–278.

Chawakitchareon, P., & Veesommaia, C. (2013). Geopolymer mortar production using silica waste as raw material. *American Transactions on Engineering & Applied Sciences, 2*(1), 3–13.

Cheng, T. W., Lee, M. L., Ko, M. S., Ueng, T. H., & Yang, S. F. (2012). The heavy metal adsorption characteristics on metakaolin-based geopolymer. *Applied Clay Science, 2012*(V56), 90–96.

Chergui, A., Bakhti, M. Z., Chahboub, A., Haddoum, S., Selatnia, A., & Junter, G. A. (2007). Simultaneous biosorption of Cu2+, Zn2+ and Cr6+ from aqueous solution by Streptomyces rimosus biomass. *Desalination, 206*(1–3), 179–184.

Chong, A. M., Wong, Y. S., & Tam, N. F. (2000). Performance of different micro-algal species in removing nickel and zinc from industrial wastewater. *Chemosphere, 41*(1–2), 251–257.

Dada, A. O., Olalekan, A. P., Olatunya, A. M., & Dada, O. (2012). Langmuir, Freundlich, Temkin and Dubinin–Radushkevich isotherms studies of equilibrium sorption of Zn unto phosphoric acid modified rice husk. *IOSR Journal of Applied Chemistry, 3*(1), 38–45.

De Weerdt, K. (2011). Geopolymers—state of the art COIN—Concrete Innovation Centre (COIN) Project report 37. ISBN 978–82–536–1251–5.

Depci, T., Kul, A. R., & Önal, Y. (2012). Competitive adsorption of lead and zinc from aqueous solution on activated carbon prepared from Van apple pulp: study in single- and multisolute systems. *Chemical Engineering Journal, 200–202*, 224–236.

Detphan, S., & Chindaprasirt, P. (2009). Preparation of fly ash and rice husk ash geopolymer. *International Journal of Minerals, Metallurgy, and Materials, 16*(6), 720–726.

Dimitrios, P., Giannopoulou, I. P., & Perraki, T. (2007). Effect of synthesis parameters on the mechanical properties of fly ash-based geopolymers. *Colloid and Surface A:Physicochemical and Engineering Aspects, 301*(1–3), 246–254.

Donat, R., Akdogan, A., Erdem, E., & Cetisli, H. (2005). Thermodynamics of Pb2+ and Ni^{2+} adsorption onto natural bentonite from aqueous solutions. *Journal of Colloid and Interface Science, 286*(1), 43–52.

El-Eswed, B., & Yousef, R. I. (2012). The effect of chemical and thermal treatments on the buffering capacity of phillipsite tuff. *Jordan Journal of Earth and Environmental Sciences, 4*(2), 7–14.

El-Eswed, B., Alshaaer, M., IbrahimYousef, R., Hamadneh, I., & Khalili, F. (2012). Adsorption of Cu(II), Ni(II), Zn(II), Cd(II) and Pb(II) onto kaolin/zeolite-based geopolymers. *Advances in Materials Physics and Chemistry, 2*, 119–125.

EPA (U.S. Environmental Protection Agency), 1991. Site characterization for subsurface remediation. EPA/625/4-91/026, Office of Research and Development, U.S. Environmental Protection Agency, Cincinnati, Ohio

Fan, T., Liu, Y., Feng, B., Zeng, G., Yang, C., Zhou, M., Zhou, H., Tan, Z., & Wang, X. (2008). Biosorption of cadmium (II), zinc (II) and lead (II) by penicillium simplicissimum: isotherms, kinetics and thermodynamics. *Journal of Hazardous Materials, 160*(2–3), 655–661.

Ferone, C., Colangelo, F., Roviello, G., Asprone, D., Menna, C., Balsamo, A., Prota, A., Cioffi, R., & Manfredi, G. (2013). Application-oriented chemical optimization of a Metakaolin based geopolymer. *Materials, 2013*(6), 1920–1939.

Foo, K. Y., & Hameed, B. H. (2010). Insights into the modeling of adsorption isotherm systems. *Chemical Engineering Journal, 156*(1), 2–10.

Ghomri, F., Lahsini, A., Laajeb, A., & Addaou, A. (2013). The removal of heavy metal ions (copper, zinc, nickel and cobalt) by natural bentonite. *Larhyss Journal, 12*, 37–54.

Hardjito, D., Wallah, S. E., Sumajouw, D. M. J., & Rangan, B. V. (2005). Fly ash-based geopolymer concrete. *Australian Journal of Structural Engineering, 2005*(6), 1–9.

Harja, M., Buema, G., Sutiman, D., & Cretescu, I. (2013). Removal of heavy metal ions from aqueous solutions using low-cost sorbents obtained from ash. *Chemical Paper, 67*(5), 497–508.

Hasar, H., Cuci, Y., Obek, E., & Dilekoglu, M. F. (2003). Removal of zinc(II) by activated carbon prepared from almond husks under different conditions. *Adsorption Science & Technology, 21*(9), 799–808.

Izquierdo, M., Querol, X., Davidovits, J., Antenucci, D., Nugteren, H., & Fernández-Pereira, C. (2009). Coal fly ash-slag-based geopolymers: microstructure and metal leachin. *Journal of Hazardous Materials, 166*(1), 561–566.

Kaya, A., & Oren, A. H. (2005). Adsorption of zinc from aqueous solutions to bentonite. *Journal of Hazardous Materials, 125*(1–3), 183–189.

Kazmi, M., Feroze, N., Javed, H., Zafar, M., & Ramzan, N. (2012). Biosorption of copper (II) on dry fruit by product: characterization, kinetic and equilibrium studies. *Journal of the Chemical Society of Pakistan, 34*(6), 156–1365.

Khalili Fawwaz, I., Salameh, N. H., & Shaybe, M. M. (2013). Sorption of uranium(VI) and thorium(IV) by Jordanian bentonite. *Journal of Chemistry.* http://www.hindawi.com/journals/jchem/2013/586136/.

Krol, M., Morawska, J., Mozgawa, W., & Pichor, W. (2014). Low temperature synthesis of zeolite from perlite waste—part I: review of methods and phase compositions of resulting products. *Materials Science-Poland, 32*(3), 503–513.

Kumar, S., Mishra, A. K., Dhanesh, S., Upadhyay, M., & Sujata, K. (2014). Adsorption studies of fly ash for removing Cu(II) from aqueous solution. *International Journal of Chemical Studies, 1*(6), 42–52.

Lancellotti, I., Kamseu, E., Barbieri, L., Corradi, A., & Leonelli, C. (2015). Municipal solid waste incinerator fly ash to obtain geopolymers. http://www.srcosmos.gr/srcosmos/showpub.aspx?aa=13176.

Li, L., Wang, S., & Zhu, Z. (2006). Geopolymeric adsorbents from fly ash for dye removal from aqueous solution. *Journal of Colloid and Interface Science, 300*(1), 52–9.

Mane, S., & Jadhav, H. S. (2008). Investigation of geopolymer mortar and concrete under high temperature. *International Journal of Emerging Technology and Advanced Engineering, 2*(12), 384–390.

Meroufel, B., Benali, O., Benyahia, M., Zenasni, M. A., Merlin, A., & George, B. (2013). Removal of Zn (II) from aqueous solution onto Kaolin by batch design. *Journal of Water Resource and Protection, 2013*(5), 669–680.

Mishra, P. C., & Patel, R. K. (2009). Removal of lead and zinc ions from water by low cost adsorbents. *Journal of Hazardous Materials, 168*(1), 319–25.

Misra, A., Gupta, R., & Gupta, R. C. (2003). Utilization of marble slurry in construction materials, workshop on gainful utilization of marble slurry and other stone waste. *Indian School of Mines.* available from: http://www.cdosindia.com.

Mon J, Deng, Y., Flury, M., & Harsh, J. B. (2005) Cesium incorporation and diffusion in cancrinite, sodalite, zeolite, and allophane. *Microporous and Mesoporous Materials 86*(1–3) 28, 277–286.

Nikolići, I., Đurović, D., Tadić, M., Blečić, D., & Radmilović, V. (2013). Immobilization of zinc from metallurgical waste and water solutions using geopolymerization technology. *Proceedings of the 16th International Conference on Heavy Metals in the Environment, Rome, Italy.*

Nriagu, J. (2007) Zinc Toxicity in Humans, elsevier publishing, http://www.extranet.elsevier.com/homepage_about/mrwd/nvrn/Zinc%20Toxicity%20in%20Humans.pdf. Accessed 28 February 2016.

Onisei, S., Pontikes, Y., Van Gervenc, T., Angelopoulos, G. N., Velea, T., Predica, V., & Moldovana, P. (2012). Synthesis of inorganic polymers using fly ash and primary lead slag. *Journal of Hazardous Materials, 205–206*(2012), 101–110.

OSHA (Occupational Safety and Health Standards). (2015). Occupational Safety and Health Administration; Washington, DC, USA: 200329CFR 1910.1000, Table Z-1.

Ozdemir, G., Ceyhan, N., Ozturk, T., Akirmak, F., & Cosar, T. (2004). Biosorption of chromium(VI), cadmium(II) and copper(II) by Pantoea sp. TEM 18. *Chemical Engineering Journal, 102*(3), 249–253.

Panias, D., & Giannopoulou, I. P. (2006). Development of inorganic polymeric materials based on fired coal fly ash. *Acta Metallurgica Slovaca, 12*(2006), 321–327.

Plum, L. M., Lothar, R., & Hajo, H. (2010). The essential toxin: impact of zinc on human health. *International Journal of Environmental Research and Public Health, 7*(4), 1342–1365.

Provis, J. L. (2006). Modeling the formation of geopolymer. PhD thesis, University of Melbourne, Australia.

Puranik, P. R., & Paknikar, K. M. (1999). Influence of co-cations on biosorption of lead and zinc—a comparative evaluation in binary and multimetal systems. *Bioresource Technology, 70*(3), 269–276.

Ramachandran, V., & D'Souza, S. F. (2013). Adsorption of nickel by Indian soils. *SF Journal of Soil Science and Plant Nutrition, 13*(1), 165–173.

Rangan, B. V. (2008). Low-calcium fly ash-based geopolymer concrete, chapter 26. In E. G. Nawy (Ed.), *Concrete construction engineering handbook* (2nd ed., pp. 26.1–26.20). New York: CRC Press.

Rushdi I. Y., Bassam E., Mazen A., Fawwaz K., & Hani K. (2009). The influence of using Jordanian natural zeolite on the adsorption, physical, and mechanical properties of geopolymers products. *Journal of Hazardous Materials, 165*(1), 379–387.

Saeed, A., Akhter, M. W., & Iqbal, M. (2005). Removal and recovery of heavy metals from aqueous solution using papaya wood as a new biosorbent. *Separation and Purification Technology, 45*, 25–31.

Saha, P., & Chowdhury, S. (2015) Insight into adsorption thermodynamics, chapter 16: edited by Tadashi Mizutani, Intech Open Access Publisher. http://cdn.intechopen.com/pdfswm/13254.pdf.

Salim, R., Al-Subu, M., Abu-Shqair, I., & Braik, H. (2003). Removal of zinc from aqueous solutions by dry plant leaves. *Trans I ChemE, 81*(Part B), 236–242.

Sampranpiboon, P., Charnkeitkong, P., & Feng, X. (2014). Equilibrium isotherm models for adsorption of zinc (II) ion from aqueous solution on pulp waste. *Wseas Transactions on Environment and Development, 10*, 35–47.

Shahmohammadi-Kalalagh, S. H., & Babazadeh, H. (2014). Isotherms for the sorption of zinc and copper onto kaolinite: comparison of various error functions. *International journal of Environmental Science and Technology, 11*(1), 111–118.

Sharmaa, P., Binoy, K., Saikia, B., & Das, M. R. (2014). Removal of methyl green dye molecule from aqueous system using reduced graphene oxide as an efficient adsorbent: kinetics, isotherm and thermodynamic parameters. *Colloids and Surfaces A: Physicochemical. Eng. Aspects, 457*, 125–133.

Shobana, R., Arockia, S. P., Dharmalingam, V., & Soruba, R. (2014). Adsorption study on zinc (II) ions from aqueous solution using chemically activated fruit of Kigelia Pinnata (JACQ) DC carbon. *International Research Journal of Environment, 3*(9), 65–69.

Sismanoglu, T, Ercag, A., Pura, S., & Ercag, E. (2004). Kinetics and isotherms of dazomet adsorption on natural adsorbents. *Journal of Brazilian Chemical Society 15*, (5). online, http://www.scielo.br/scielo.php?script=sci_arttext&pid=S0103-50532004000500010.

Solomon Samu, J., Martin Devaprasath, P., & Chandramohan, M. (2012). Removal of Cu (II) from aqueous solution by using natural plant material Cynodon dactylon. *Research Journal of Pharmaceutical, Biological and Chemical Sciences, 3*(2), 304–321.

Srivastava, S., Chaudhary, R., & Khale, D. (2008). Influence of pH, curing time and environmental stress on the immobilization of hazardous waste using activated fly ash. *Journal of Hazardous Materials, 153*(3), 1103–1109.

Swanepoel, J. C., Strydom, C. A., Swanepoel, J. C., & Strydom, C. A. (2002). Utilization of fly ash in a geopolymeric material. *Applied Geochemistry, 17*, 1143–1148.

Tahir, S., & Naseem, R. (2007). Removal of Cr(III) from tannery wastewater by adsorption onto bentonite clay. *Separation and Purification Technology, 53*, 312–321.

van Jaarsveld, J. G., van Deventer, J. S., & Lukey G. (1989) The effect of composition and temperature on the properties of fly ash- and kaolinite-based geopolymers. *Chemical Engineering Journal 89* (1–3), 63–73.

Van Jaarsveld, J. G. S., Van Deventer, J. S. J., & Lorenzen, L. (1997). The potential use of geopolymeric materials to immobilise toxic metals: part I. theory and applications. *Mineral Engineering, 10*(7), 659–669.

Wahi, R., Kanakaraju, D., & Yusuf, N. A. (2010). Preliminary study on zinc removal from aqueous solution by sago wastes. *Global Journal of Environmental Research, 4*(2), 127–134.

Wang, S., Li, L., & Zhu, Z. H. (2007). Solid-state conversion of fly ash to effective adsorbents for Cu removal from wastewater. *Journal of Hazardous Materials, 139*(2), 254–259.

Wasewar K. L., Atif, M., Prasad, B., & Mishra, I. M. (2009). Batch adsorption of Zn using tea factory waste as an adsorbent. *Desalination, 244*(1–3), 66–71.

Wasewar, K. L., Mohammad, A., & Prasad, B. (2008). Characterization of factory tea waste as an adsorbent for removal of heavy metals. *Jornal of Future Engineering Technonlogy, 3*(3), 47–53.

Wu, D., Sui, Y., He, S., Wang, X., Li, C., & Kong, H. (2008). Removal of trivalent chromium from aqueous solution by zeolite synthesized from coal fly ash. *Journal of Hazardous Materials, 155*(3), 415–423.

Xu, H., van Deventer, J. S. J., & Lukey, G. C. (2001). Effect of alkali metals on the preferential geopolymerization of stilbite/kaolinite mixtures. *Industrial & Engineering Chemistry Research, 40*(17), 3749–3756.

Xu, H., Jannie, S. J., & Deventer, V. (2002). Geopolymerisation of multiple minerals. *Minerals Engineering, 15*(12), 1131–1139.

Yan G., & Viraraghavan T. (2003) Heavy-metal removal from aqueous solution by fungus Mucor rouxii. *Water Research, 37*(18), 4486–96.

Yun-Guo, L., Ting, F., Guang-ming, Z., Xin, L., Qing, T., Fe, Y., Ming, Z., Wei-hua, X., & Yu-e, H. (2006). Removal of cadmium and zinc ions from aqueous solution by living Aspergillus niger. *Transactions of Nonferrous Metal Society China, 16*, 681–686.